Nonadiabatic interaction effects in the spectra of ultralong-range Rydberg molecules

Rohan Srikumar,[1,*] Frederic Hummel,[2,†] and Peter Schmelcher[1,3,‡]

[1]*Zentrum für Optische Quantentechnologien, Fachbereich Physik, Universität Hamburg, Luruper Chaussee 149, 22761 Hamburg, Germany*

[2]*Max-Planck-Institut für Physik Komplexer Systeme, Nöthnitzer Straße 38, 01187 Dresden, Germany*

[3]*The Hamburg Centre for Ultrafast Imaging, Universität Hamburg, Luruper Chaussee 149, 22761 Hamburg, Germany*

(Received 1 February 2023; revised 6 June 2023; accepted 7 June 2023; published 14 July 2023)

Ultralong-range Rydberg molecules (ULRMs) are highly imbalanced bound systems formed via the low-energy scattering of a Rydberg electron with a ground-state atom. We investigate for ^{23}Na the d state and the energetically close-by trilobite state, exhibiting avoided crossings that lead to the breakdown of the adiabatic Born-Oppenheimer (BO) approximation. We develop a coupled-channel approach to explore the nonadiabatic interaction effects between these electronic states. The resulting spectrum exhibits stark differences in comparison to the BO spectra, such as the existence of above-threshold resonant states without any adiabatic counterparts, and a significant rearrangement of the spectral structure as well as the localization of the eigenstates. Our study motivates the use of ^{23}Na ULRMs, as a probe to explore vibronic interaction effects on exaggerated timescales and length scales.

DOI: 10.1103/PhysRevA.108.012809

I. INTRODUCTION

Rydberg atoms are an important player in modern quantum physics due to their unique and extreme properties. Their size and dipole moment scale as n^2, and lifetimes and polarizability scale as n^3 and n^7, respectively, where n is the principal quantum number [1,2]. They offer a state-dependent interaction strength and enhanced sensitivity to electromagnetic fields, rendering them promising platforms for quantum computing [3–7], external field sensing [8–10], detection of polar molecules [11–13], and Rydberg-quantum optics [14–17]. The pioneering article in [18] predicted the formation of ultralong-range Rydberg molecules (ULRMs), as a result of attractive scattering interaction of the Rydberg electron with a ground-state perturbing atom. These exotic bound states feature permanent dipole moments of the order of kilodebye and bond lengths of the order of micrometers, properties which were unheard of in conventional diatomic molecules. However, recent works have also studied other exotic bound molecular systems with exaggerated properties, formed due to different binding mechanisms like the Rydberg macrodimer [19–21] and the Rydberg atom-ion molecule [22–27].

This work is dedicated to the diatomic ULRM, bound as a consequence of low-energy electron-atom s-wave scattering. The scattering mechanism enables the existence of two distinct classes of molecular states [18]. The first type is formed when a Rydberg electron of low angular momentum ($l \leqslant 2$) interacts with the neutral perturber. Molecules of the low-l class exhibit shallow potential wells (approximately 10 MHz) and a very small net electronic dipole moment [28]. The second type is the trilobite class of molecules [29,30], which arise as the high-l hydrogenic manifold is mixed by the ground-state atom [31]. The trilobite molecules exhibit much deeper potential wells (on the order of gigahertz) and a large permanent dipole moment and is responsible for garnering much interest to the field of ULRMs. In addition, the use of higher-order terms in our scattering interaction has also demonstrated the existence of the butterfly state [32,33], which arises as a consequence of p-wave shape resonances. More recently, detailed theoretical models that include higher partial waves of the electron-atom scattering interaction have also been constructed [34]. Starting from its experimental observation in [35], significant progress have been made in the study of ULRMs over the past two decades. This includes its utility, as a probe for spatial correlations in ultracold atomic gases [36], in precision spectroscopy of negative-ion resonance [37], and in the study of Rydberg impurities in ultracold atomic gases [38,39]. Furthermore, the fine and hyperfine structures of these molecules [40–42] as well as their behavior in external electric and magnetic fields have been studied [43–47], and major strides have been made in the experimental exploration of these molecules (see [33,35,37,48–59] for examples of experimental investigations on ULRMs).

One of the important theoretical tools used in the analysis of a ULRM is the well-established Born-Oppenheimer (BO) approximation [60]. As a cornerstone of molecular physics, the BO approximation advocates for the separation of slow nuclear and fast electronic motion, allowing us to independently solve the electronic problem in varying geometrical arrangements of the nuclei, to obtain the so-called adiabatic potential energy curves (PECs). However, there is typically a ubiquity of avoided crossings featured in the PECs of the ULRM and resultingly nonadiabatic interactions potentially leading to the breakdown of the BO approximation are expected. Such a breakdown of adiabaticity can result in the

*rsrikuma@physnet.uni-hamburg.de
†hummel@pks.mpg.de
‡pschmelc@physnet.uni-hamburg.de

altered spectra and lifetimes of molecular states and even introduce metastable states that are subject to nonadiabatic decay [61]. In the special case of a conical intersection (CI), when the molecular geometry facilitates the degeneracy of two PECs, the nonadiabatic couplings become singular and the adiabatic approximation breaks down completely [62–66]. Recent studies have demonstrated the existence of such CIs in the Rb ULRM, for very specific conditions, when the electron-perturber scattering phase shift divided by π is similar in size to the quantum defect, i.e., $\mu_d \pi \approx \delta_s$ [67]. In the context of traditional molecular physics, CIs play an important role in molecular dynamics as they can cause fast nonradiative transitions between electronic states [68–71], Jahn-Teller distortions [72,73], and surface hoppings [74,75], to name a few examples. The study of nonadiabatic effects in the vicinity of conical intersections has been proven to be necessary for understanding a wide range of natural phenomena such as photostability of DNA [76,77], photoisomerization [78,79], and reaction mechanisms involving photosynthesis [80]. The ULRM, on the other hand, provides us with a platform to explore molecular dynamics in the unique and enormous timescales of microseconds and on length scales of micrometers. Hence, the study of nonadiabatic interaction effects, as well as their contribution to the spectral characteristics in a molecule which features such exaggerated properties, is a challenging and promising direction of research on ULRMs. It is of relevance to mention that recent studies of the Rydberg macrodimer and the Rydberg atom-ion molecule also consider nonadiabatic interaction effects, enabling us to theoretically explore beyond BO physics in multiple exotic Rydberg systems [20,22,81].

In this work we focus on the nonadiabatic interaction between two electronic states in ^{23}Na ULRMs, due to the vibronic coupling between them. The electronic level structure of ^{23}Na leads to avoided crossings and state mixing between the trilobite and the d-state PECs (see [82], for a recent study on vibronic couplings between trilobite and butterfly states). The onset of prominent vibronic interaction effects, as a result of the aforementioned electronic level structure, justifies the choice to study sodium as opposed to heavier atoms. We highlight results for specific n values, with near-degenerate avoided crossings that cause singular vibronic couplings, explained using the concept of CIs in synthetic dimensions. A coupled-channel approach is employed to obtain the vibronic spectra, thereby using the nonadiabatic couplings between the trilobite and d-state PECs. We observe features of vibronic interactions in the underlying spectra including scattering resonance states with no adiabatic counterparts. We also use the single-channel Born-Huang approximation, including the nonadiabatic diagonal corrections without the off-diagonal couplings as a comparative resource. The analysis of vibronic and vibrational spectra is used to justify the necessity of a coupled-channel approach to study the ^{23}Na ULRM.

This work is organized as follows. Section II contains the theory and methodology used throughout this work. Section II A elaborates on the general molecular Hamiltonian and gives insight into the approximations and terminology used to study nonadiabatic couplings. Section II B focuses on the electronic interactions in the ULRM and introduces the electronic states and PECs relevant to our work, before we discuss the specific two-level system and the problem of diabatization in Secs. II C and II D, respectively. The computational tools used as well as the approach to obtain the vibronic spectra are discussed in Sec. III. Section IV features the results and discussion. Section IV is further divided into Sec. IV A, addressing the electronic structure of the ^{23}Na ULRM; Sec. IV B, discussing the nonadiabatic couplings; and Sec. IV C, providing a comparative analysis of the coupled-channel vibronic spectrum and the single-channel approximations. A summary and outlook are presented in Sec. V.

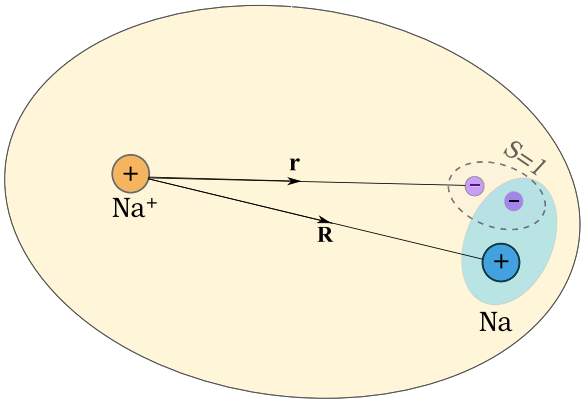

FIG. 1. Sketch of the ^{23}Na ULRM, illustrating the scattering interaction between the Rydberg electron at position **r** and the ground-state atom at position **R**. The triplet nature of the scattering interaction is highlighted.

II. THEORY AND METHODOLOGY

In this section we present the Hamiltonian governing the internal molecular dynamics of the ULRM and the corresponding Schrödinger equation in atomic units. We then proceed to elaborate on the nonadiabatic features of our system and the approximations used to circumvent them. Later we introduce the scattering interaction which forms the binding mechanism of the ULRM and discuss the electronic spectra of the molecule. The focus is then shifted to the interaction between the trilobite and the d state, and the vibronic coupling between them. Finally, we introduce the concept of diabatization and use it in our two-state system as a precursor to obtaining the vibronic spectra.

A. Hamiltonian, adiabatic separation, and nonadiabatic couplings

Our system consists of two ^{23}Na atoms, one in the Rydberg state and the other one in the ground state. Transforming the two-atom system into relative coordinates, **R** is the internuclear vector of the two atoms and **r** is the Rydberg electron position, with the ionic core at the coordinate origin, as depicted in Fig. 1. The Rydberg electrons' interactions with the parent core and the ground-state perturber, as well as the vibrational motion of the diatomic system, are captured in the

molecular single-electron effective Hamiltonian

$$\mathbf{H}_{\rm m} = \frac{\mathbf{P}_{\rm nu}^2}{2\mu} + \underbrace{\frac{\mathbf{p}_{\rm e}^2}{2\mu_{\rm e}} + V_{\rm Ryd}(\mathbf{r}) + V_{en}(\mathbf{R},\mathbf{r})}_{\mathbf{H}_{\rm e}(\mathbf{R},\mathbf{r})}. \tag{1}$$

The first term represents the nuclear kinetic energy $T_{\rm nu}$ along the vibrational degree of freedom, the second term and the third term represent the kinetic energy of the Rydberg electron $T_{\rm e}$ and its interaction with the Rydberg ionic core $V_{\rm Ryd}$, respectively, and the last term V_{en} represents the electron-perturber interaction. In addition, μ and $\mu_{\rm e}$ are the reduced masses of the two nuclei and the electron, respectively. Isolating $\mathbf{H}_{\rm e}(\mathbf{R},\mathbf{r})$ as the electronic Hamiltonian which is parametrically dependent on the internuclear coordinate, we could solve for the corresponding electronic problem. The resulting eigenvalues, i.e., the PECs $\varepsilon_i(\mathbf{R})$ and eigenvectors $\psi_i(\mathbf{R},\mathbf{r})$, depend parametrically on the internuclear coordinates and we have

$$\mathbf{H}_{\rm e}(\mathbf{R},\mathbf{r})\,|\psi_i(\mathbf{R},\mathbf{r})\rangle = \varepsilon_i(\mathbf{R})\,|\psi_i(\mathbf{R},\mathbf{r})\rangle\,. \tag{2}$$

The total molecular wave function can be expanded using the electronic eigenfunctions according to $\Psi_{\rm m}(\mathbf{R},\mathbf{r}) = \sum_i \chi_i(\mathbf{R})\psi_i(\mathbf{R},\mathbf{r})$, known as the Born-Oppenheimer expansion [60,83]. It is an exact representation of the molecular wave function, as the electronic eigenfunctions form an orthonormal and complete basis. Here $\{\chi_i(\mathbf{R})\}$ are the expansion coefficients which portray the $\mathbf{R}$-dependent mixing of electronic states. Inserting this expansion into the molecular Schrödinger equation $\mathbf{H}_{\rm m}\Psi_{\rm m} = E\Psi_{\rm m}$ and integrating out the electronic degrees of freedom, we obtain the coupled-channel time-independent Schrödinger equation (TISE) for the vibrational motion [62]

$$-\frac{1}{2\mu}\nabla_{\mathbf{R}}^2\chi_i(\mathbf{R}) + \varepsilon_i(\mathbf{R})\chi_i(\mathbf{R}) - \frac{1}{2\mu}\sum_j \Lambda_{ij}(\mathbf{R})\chi_j(\mathbf{R}) = E\,\chi_i(\mathbf{R}). \tag{3}$$

Here Λ_{ij} are the nonadiabatic couplings between the nuclear and electronic motions, which can be written as

$$\Lambda_{ij} = 2P_{ij}\nabla_{\mathbf{R}} + Q_{ij}, \tag{4}$$

where $P = (P_{ij})$ and $Q = (Q_{ij})$ are the first- and second-order derivative couplings, defined as

$$P_{ij} = \langle\psi_i(\mathbf{R},\mathbf{r})|\nabla_{\mathbf{R}}|\psi_j(\mathbf{R},\mathbf{r})\rangle\,, \tag{5}$$

$$Q_{ij} = \langle\psi_i(\mathbf{R},\mathbf{r})|\nabla_{\mathbf{R}}^2|\psi_j(\mathbf{R},\mathbf{r})\rangle\,, \tag{6}$$

where angular brackets denote the integration with respect to the electronic degrees of freedom. Here P and Q essentially introduce the coupling between different electronic states ψ_i and ψ_j due to the motion of the nuclei, which in turn affects the vibrational motion of the nuclei. Once the P matrix is obtained, it is straightforward to calculate the second-order coupling using the relation

$$Q_{ij} = \nabla_{\mathbf{R}}P_{ij} + P_{ij}^2, \tag{7}$$

where

$$P_{ij}^2 = -\langle\nabla_{\mathbf{R}}\psi_i(\mathbf{R},\mathbf{r})|\nabla_{\mathbf{R}}\psi_j(\mathbf{R},\mathbf{r})\rangle\,. \tag{8}$$

It is possible to write Eq. (3) in a more compact way, using the complete P matrix as

$$-\frac{1}{2\mu}(\nabla_{\mathbf{R}} + P)^2\boldsymbol{\chi}(\mathbf{R}) + \varepsilon(\mathbf{R})\boldsymbol{\chi}(\mathbf{R}) = E\,\boldsymbol{\chi}(\mathbf{R}), \tag{9}$$

with the vector $\boldsymbol{\chi} = (\chi_i)$, which contains the expansion coefficients, and the diagonal potential energy matrix ε, which contains the corresponding PECs. The nonadiabatic couplings are shown to manifest as off-diagonal terms in the kinetic energy operator for the nuclear vibrational motion.

The BO approximation [60,62–64,83] is used to solve Eq. (3) as a standard approximation, where the nonadiabatic terms are completely neglected, resulting in the decoupling of the molecular vibrational Schrödinger equations governing χ_i to form

$$-\frac{1}{2\mu}\nabla_{\mathbf{R}}^2\chi_i(\mathbf{R}) + \varepsilon_i(\mathbf{R})\chi_i(\mathbf{R}) = E_i\chi_i(\mathbf{R}). \tag{10}$$

Here the total molecular state is simply $\Psi_{{\rm m},i}(\mathbf{R},\mathbf{r}) = \chi_i(\mathbf{R})\psi_i(\mathbf{R},\mathbf{r})$, i.e., the electronic and nuclear motion are adiabatically separated. In addition, $\psi_i(\mathbf{R},\mathbf{r})$ is the adiabatic eigenstate, $\varepsilon_i(\mathbf{R})$ is the adiabatic PEC which describes the electronic motion, and $\chi_i(\mathbf{R})$ is the vibrational wave function on each PEC. These adiabatic states and energy surfaces can be obtained by solving $\mathbf{H}_{\rm e}$ at each fixed nuclear geometry. Equation (10) then describes the vibrational motion of each individual adiabatic potential energy curve. The adiabatic approximation can be justified due to the large differences in masses between the electrons and the nuclei, resulting in very different timescales of their motions. Hence the nuclei are approximated to remain frozen over the course of the electronic dynamics.

In a second approximation, called the Born-Huang (BH) approximation [84–86], we include the diagonal derivative coupling operator Λ_{ii} in Eq. (10),

$$-\frac{1}{2\mu}\nabla_{\mathbf{R}}^2\chi_i(\mathbf{R}) + \varepsilon_i^b(\mathbf{R})\chi_i(\mathbf{R}) = E_i\chi_i(\mathbf{R}), \tag{11}$$

where

$$\varepsilon_i^b(\mathbf{R}) = \varepsilon_i(\mathbf{R}) - \frac{1}{2\mu}\Lambda_{ii}(\mathbf{R}). \tag{12}$$

The Born-Huang approximation still maintains the decoupling between different adiabatic electronic states due to nuclear motion; instead it merely adds a correction to each isolated PEC due to the finite kinetic energy of the nuclei. Hence the BH approximation, much like the BO approximation, results in a single-channel TISE by ignoring the off-diagonal couplings of the coupled-channel TISE (3). The nomenclature used here is based on works in nonadiabatic molecular physics [85,86] and is not to be confused with the notion of a Born-Huang expansion or other potentially ambiguous terminology. Note that P is anti-Hermitian, whereas Q is non-Hermitian. Hence, if the electronic eigenfunctions are real, P_{ii}, the diagonal first-order term vanishes and we obtain $(\Lambda_{ii} = Q_{ii}) \leqslant 0$ [from Eqs. (7) and (8)], thereby causing a purely positive shift in the adiabatic PEC.

Both the Born-Oppenheimer and Born-Huang approximations are valid only when the $\mathbf{R}$ dependence of ψ_i and ε_i is adiabatic, i.e., the change of electronic motion with respect

to **R** is gradual. However, both of these assumptions are broken in the vicinity of an avoided level crossing of two PECs, where the coupling between the electronic states is nonnegligible due to a high **R** sensitivity of the electronic states. The strong vibronic coupling effects between the vibrational and electronic states, due to the avoided crossings, can change the spectra and lifetimes of molecules and facilitate surface hopping across the avoided crossing.

B. Electronic interaction

Solving the molecular Hamiltonian for a ULRM first requires the characterization of the electronic interaction between the Rydberg electron and ground-state atom, which perturbs the Rydberg electron wave function via low-energy scattering. We model V_{en}, the interaction potential, using a Fermi pseudopotential [87,88] for s-wave scattering,

$$V_{en}(\mathbf{r},\mathbf{R}) = 2\pi a_s^T(k)\delta(\mathbf{r}-\mathbf{R}), \tag{13}$$

where $a_s^T(k) = a_s^T(0) + \pi\alpha k/3$ is the energy-dependent triplet s-wave scattering length for electron collisions with ground-state atoms, where $a_s^T(0) = -5.9$ is the zero-energy triplet scattering length [89,90] and $\alpha = 162.7$ is the polarizability [91–93]. The wave number k can be semiclassically determined using $k^2 = 2/R - 1/n^2$. The negative triplet scattering length facilitates an attractive interaction capable of binding the two ^{23}Na atoms. A pictorial representation of the interaction is presented in Fig. 1.

The adiabatic electronic Hamiltonian for the ULRM is hence given by $H_e = H_{\rm Ryd} + V_{en}$, where $H_{\rm Ryd}$ is the Rydberg electron Hamiltonian. The H_e can be diagonalized in the Rydberg-state basis $\{\langle\mathbf{r}|nlm\rangle = \phi_{nlm}(\mathbf{r})\}$, which satisfies the Rydberg atom's TISE

$$H_{\rm Ryd}\,|nlm\rangle = -\frac{1}{2(n-\mu_l)^2}\,|nlm\rangle\,, \tag{14}$$

where $|nlm\rangle$ is an atomic Rydberg eigenstate. In our case μ_l is the l-dependent quantum defect of ^{23}Na [67,94], which determines the detuning of each quantum-defect state with reference to the hydrogenic state with energy $E_n = -1/2n^2$. It is worth noting that we omit the fine and hyperfine structures of the atomic Rydberg Hamiltonian. These terms may indeed be relevant for specific systems and consequently cannot be ignored if the aim is a comparison with (precise) spectroscopic experimental data. However, our goal is to provide evidence for the vibronic interaction effects primarily and hence we focus purely on the binding interaction, but acknowledge the necessity to introduce further interactions depending on the considered case and species. The spherical symmetry of the Hamiltonian implies that, without loss of generality, the internuclear axis can be taken as the z axis and only $m = 0$ states contribute. The high-angular-momentum states ($n-1 \geqslant l \geqslant 3$ for Na) are approximately degenerate to the hydrogenic manifold due to negligible quantum defects. Degenerate perturbation theory is used to obtain the high-l adiabatic electronic states of H_e,

$$|t\rangle = \frac{1}{T}\sum_{l=3}^{n-1}\phi_{nl0}(R\hat{\mathbf{z}})\phi_{nl0}(\mathbf{r}), \tag{15}$$

where

$$T^2 = \sum_{l=3}^{n-1}|\phi_{nl0}(R\hat{\mathbf{z}})|^2, \tag{16}$$

and the corresponding potential energy curve

$$t(R) = 2\pi a_s^T(k)T^2, \tag{17}$$

which are popularly known as the trilobite state and trilobite PEC [18,31,41]. The low-angular-momentum Rydberg-electron states ($l < 3$) are energetically far detuned from the hydrogenic manifold due to significant quantum defects. Using nondegenerate perturbation theory, we obtain the isolated low-l adiabatic electronic state of H_e,

$$|q\rangle = \phi_{\nu l0}(\mathbf{r}) \tag{18}$$

and the corresponding potential energy curve

$$q(R) = 2\pi a_s^T(k)|\phi_{\nu l0}(R\hat{\mathbf{z}})|^2, \tag{19}$$

where $\nu = n - \mu_l$ is the effective principal quantum number. Note that the low-l molecular electronic state is essentially the Rydberg-electron state, without any R-dependent state mixing. These two PECs, first introduced in [18], are the building blocks of the Rydberg ULRM. The trilobite PECs feature wells which are significantly deeper (on the order of gigahertz) than their low-l counterparts (on the order of megahertz) and can support multiple bound molecular states. These trilobite molecules are extremely polar with a large electric dipole moment $D \approx R - n^2/2\,ea_0$ (a_0 is the length scale in atomic units) as compared to the nonpolar low-l molecules, which can only support a few weakly bound states. This simple perturbative method covers the fundamental properties of Rydberg molecules and it allows us to study the two distinct classes of PECs and analyze the properties of both polar and nonpolar molecules formed by them.

C. Two-level system

As a prototype setup, the nonadiabatic interactions in ^{23}Na ULRMs can be effectively probed by studying the interaction between the trilobite and $l = 2$, i.e., the d quantum-defect state relevant in sodium. We expand H_e in a restricted basis $\{|t\rangle\,, |q\rangle\}$ consisting of the trilobite and d state to obtain

$$V_e = \begin{bmatrix}\langle t|H_e|t\rangle & \langle q|H_e|t\rangle \\ \langle t|H_e|q\rangle & \langle q|H_e|q\rangle\end{bmatrix} = \begin{bmatrix} t & \sqrt{qt} \\ \sqrt{qt} & q+\Delta\end{bmatrix}, \tag{20}$$

where Δ is the energy splitting between the d state with reference to the hydrogenic manifold. Note that the notation used is based on [67], for the sake of continuity and convenience, but the inner product of two eigenstates is summed over coherently without the loss of sign information. The upcoming strategy would be to use the BO approximation and obtain the adiabatic states of the restricted two-level system and utilize them to calculate the nonadiabatic coupling terms. The behavior of these nonadiabatic terms might warrant the necessity to transform our system into a basis where the vibronic spectra can be readily calculated. Moving along our road map, two adiabatic PECs (see Fig. 2) are obtained from the diagonalization

$$V_\pm(R) = \tfrac{1}{2}[t+q+\Delta \pm \sqrt{(t-q-\Delta)^2+4qt}], \tag{21}$$

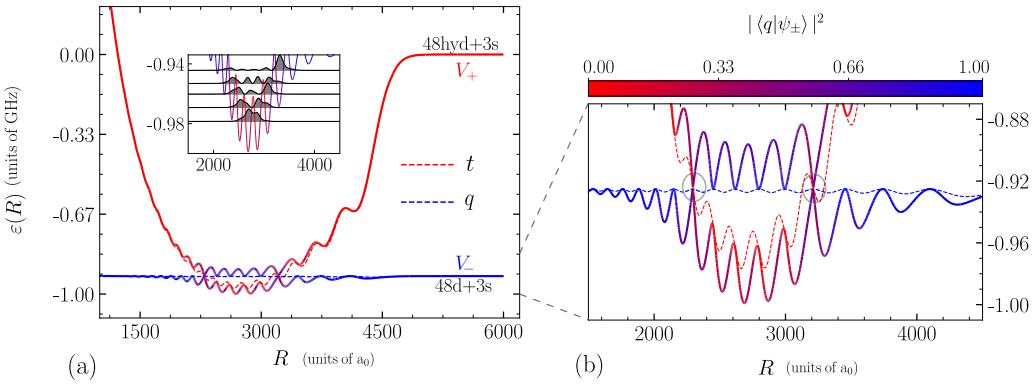

FIG. 2. (a) Adiabatic and diabatic potential energy curves for $n = 48$. The V_- and t PECs converge to the $48d$ electronic state as it approaches the dissociation limit (approximately 4500 a_0) and V_+ and q PECs converges to the $n = 48$ hydrogenic state. The inset presents the lowest five vibrational levels in the V_- PEC and their probability densities. (b) Magnified view of the region with prevalent state mixing ($2000\,a_0 \leqslant R \leqslant 4000\,a_0$). The diabatic curves are allowed to cross each other, but the adiabatic curves show nearly degenerate avoided crossings at $R \sim 2295\,a_0$ and $3210\,a_0$ (encircled regions), respectively. The color bar features the $l = 2$ character of the PECs as a function of R.

along with their corresponding adiabatic electronic states

$$\begin{aligned} |\psi_-\rangle &= \cos\theta\,|t\rangle + \sin\theta\,|q\rangle, \\ |\psi_+\rangle &= -\sin\theta\,|t\rangle + \cos\theta\,|q\rangle, \end{aligned} \tag{22}$$

where θ is the mixing angle given by

$$\theta = \arccos\left(\frac{\sqrt{qt}}{\sqrt{(V_- - t)^2 + qt}}\right). \tag{23}$$

The state mixing is largely determined by the detuning and the coupling strength. For $\Delta \gg q, t$ such that $\sqrt{qt}/(t - q - \Delta) \sim 0$, as is the case for $l < 2$, we obtain $V_\pm \approx \{q, t\}$. For large detuning the adiabatic PECs act similarly to the uncoupled d state PEC and trilobite PEC independently. Here we assume that the rotational motion of the molecule is negligible, thereby restricting the internuclear motion to the radial dimension and establishing our system as a two-level single-parameter model. The validity of this assumption relies on the fact that the extremely large internuclear distance results in an extremely narrow rotational structure (proportional to kilohertz). Hence, the dominant interaction effects visible at moderate resolution are primarily due to the coupling of electronic and vibrational motion (proportional to megahertz and gigahertz). From this two-level picture, the derivative couplings between the two adiabatic states are determined to be

$$\begin{aligned} P_{12} &= \langle\psi_-|\partial_R|\psi_+\rangle = -\theta', \\ Q_{11} &= \langle\psi_-|\partial_R^2|\psi_-\rangle = -\theta'^2 + \cos^2(\theta)\,\langle t|\partial_R^2|t\rangle, \\ Q_{22} &= \langle\psi_-|\partial_R^2|\psi_-\rangle = -\theta'^2 + \sin^2(\theta)\,\langle t|\partial_R^2|t\rangle, \end{aligned} \tag{24}$$

where

$$\langle t|\partial_R^2|t\rangle = \frac{M^4}{T^4} - \frac{B^2}{T^2}, \tag{25}$$

with $\theta' = \partial_R\theta$, $B^2 = \sum_l |\phi'_{nl0}(R)|^2$, and $M^2 = \sum_l \phi'_{nl0}(R)\phi_{nl0}(R)$.

Figure 3(a) shows the calculated derivative couplings for $n = 48$. The derivative couplings determined are prone to be divergent for certain n and R. The existence of these singularities [95] pose numerical problems in solving Eq. (3); hence it is of use to employ methods whereby the vibrational

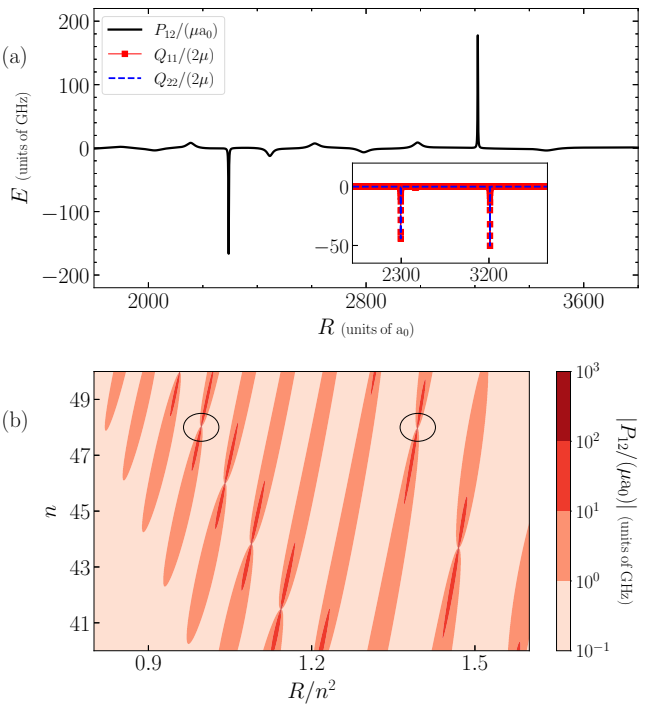

FIG. 3. Nonadiabatic couplings of the adiabatic electronic states $|\psi_-\rangle$ and $|\psi_+\rangle$. (a) First-order derivative coupling (black) P_{12}/μ for $n = 48$. The inset depicts the second-order derivative coupling $Q_{11}/2\mu$ (red) and $Q_{22}/2\mu$ (blue). Both the first- and second-order derivative couplings portray two near-singular peaks corresponding to the avoided level crossings at $R \sim 2295\,a_0$ and $3210\,a_0$, respectively. (b) Parameter scan of the magnitude of $P_{12}(n, R)$ over varying n. Multiple n values are found possessing strong nonadiabatic couplings; the peaks near $n = 48$ are encircled.

Schrödinger equation is solved without dealing with divergent derivative couplings.

D. Diabatization

The derivative coupling terms, as discussed before, manifest as off-diagonal terms based on the nuclear kinetic energy operator. The idea of diabatization [62,64] is to perform a unitary transformation which diagonalizes the kinetic energy matrix, whereby the need for derivative couplings in solving the vibrational TISE is circumvented. As a result of such a transform, off-diagonal potential energy terms may be introduced in the new basis, which accounts for the vibronic couplings in the diabatic basis. A unitary transformation $\bar{\boldsymbol{\chi}}(R) = U(R)\boldsymbol{\chi}(R)$ would transform the TISE (9) into

$$-\frac{1}{2\mu}(\mathbb{I}\partial_R + \bar{P})^2\bar{\boldsymbol{\chi}}(R) + \bar{\varepsilon}(R)\bar{\boldsymbol{\chi}}(R) = E\,\bar{\boldsymbol{\chi}}(R), \tag{26}$$

where

$$\bar{\varepsilon}(R) = U^{\dagger}\varepsilon(R)U, \quad \bar{P} = U^{\dagger}(PU + \partial_R U). \tag{27}$$

The transformed derivative coupling matrix vanishes if

$$\partial_R U = -PU, \tag{28}$$

in which case the matrix U represents the diabatic transform, and $\bar{\varepsilon}$ is the diabatic potential energy matrix with off-diagonal terms. While it may not be possible to construct such a unitary transform in all situations, for a two-level system with a single parameter R, such a transformation exists analytically [20,96] where U is a rotation about the angle,

$$\gamma(R) = \int_R^{\infty} P_{12}(R_1)dR_1. \tag{29}$$

Using the corresponding form of P_{12}, we obtain $\gamma(R) = -\int_R^{\infty}\theta'(R_1)dR_1 = -\theta(R)$. Hence, the diabatic basis is proven to be the restricted electronic basis $\{|t\rangle, |q\rangle\}$, which was used as the initial ansatz. This gives the diabatic potential matrix

$$\bar{\varepsilon} = \begin{bmatrix} t & \sqrt{qt} \\ \sqrt{qt} & q + \Delta \end{bmatrix}. \tag{30}$$

We have theoretically derived the adiabatic electronic states, nonadiabatic couplings, and the diabatic potential energy curves. What is left is to obtain the vibronic spectrum, by solving the coupled vibrational Schrödinger equations, using the given diabatic potential energy matrix, the elements of which vary as smooth functions of R, devoid of any singularities.

III. COMPUTATIONAL APPROACH: VIBRONIC STRUCTURE

Based on the diabatic PECs, we use a tenth-order finite-difference method [97] to obtain the vibrational wave functions by solving the TISE for each adiabatic PEC. Convergent eigenvalues and wave functions are observed for a grid of $1000\,a_0$–$6000\,a_0$, with a step size of $1a_0$. Convergence of P and Q demands much finer grid steps near the avoided crossings. This is overcome by diabatization; using the smooth diabatic PECs, we obtain a convergent eigenspectrum for the coupled-channel vibronic system for a step size of $1a_0$. Once the diabatic basis is obtained, the coupled-channel vibronic Hamiltonian in the diabatic basis can be represented as

$$H_{\mathrm{m}} = \begin{bmatrix} T_{\mathrm{nu}} + t(R) & \sqrt{qt}(R) \\ \sqrt{qt}(R) & T_{\mathrm{nu}} + q(R) + \Delta \end{bmatrix}, \tag{31}$$

where T_{nu} is the nuclear kinetic energy term acting on each of the diagonal PECs. Solving the TISEs $H_t = T_{\mathrm{nu}} + t(R)$ and $H_q = T_{\mathrm{nu}} + q(R)$ on the aforementioned grid gives us the eigenspectra $\{E_i^t, |\chi_i^t\rangle\}$ and $\{E_i^q, |\chi_i^q\rangle\}$ corresponding to each diagonal diabatic PEC. We can then expand any eigenvector of H_{m} as

$$\left|\Psi_{\mathrm{m}}^j\right\rangle = \sum_{i=0}^{N-1} c_i^j \left|\bar{\chi}_i^t\right\rangle |t\rangle + \sum_{i=0}^{N-1} d_i^j \left|\bar{\chi}_i^q\right\rangle |q\rangle\,, \tag{32}$$

where

$$H_{\mathrm{m}}\left|\Psi_{\mathrm{m}}^j\right\rangle = E^j\left|\Psi_{\mathrm{m}}^j\right\rangle. \tag{33}$$

Here $\{c^j\}$ and $\{d^j\}$ are expansion coefficients obtained by diagonalizing H_{m} in the diabatic basis and N is the number of vibrational states from each diagonal PEC used for diagonalization. Note that the eigenvector can no longer be separated into well-defined electronic or vibrational parts. However, tracing out the electronic degree of freedom leaves us with the vibrational probability density of $|\Psi_{\mathrm{m}}^j\rangle$ along the internuclear axis,

$$P^j(R) = \left|\bar{X}_t^j(R)\right|^2 + \left|\bar{X}_q^j(R)\right|^2, \tag{34}$$

where

$$\bar{X}_t^j(R) = \sum_{i=0}^{N-1} c_i^j\,\bar{\chi}_i^t(R), \quad \bar{X}_q^j(R) = \sum_{i=0}^{N-1} d_i^j\,\bar{\chi}_i^q(R). \tag{35}$$

The $P^j(R)$ can be compared to the probability density of the vibrational states in each adiabatic PEC (see Figs. 4 and 5), whereby differences in vibrational motion can be observed between the adiabatic and nonadiabatic cases. To observe electronic-state mixing, we transform the vibronic eigenstate back to the adiabatic basis where $\boldsymbol{X}^j = U^{\dagger}\bar{\boldsymbol{X}}^j$, where $U^{\dagger}$ is the inverse-diabatic transform, to obtain

$$\left|\Psi_{\mathrm{m}}^j\right\rangle = X_-^j(R)\,|\psi_-\rangle + X_+^j(R)\,|\psi_+\rangle\,, \tag{36}$$

where $X_{\pm}$ provides the R-dependent electronic-state mixing due to the nonadiabatic couplings, and

$$p_{\pm} = \int |X_{\pm}(R)|^2 dR, \tag{37}$$

which provides the population for the state $|\psi_{\pm}\rangle$. Color mapping the $P^j(R)$ with the population p_- (see Figs. 4 and 5) is an effective way to visualize both the electronic and vibrational contributions to each vibronic eigenstate. The unbound states above the dissociation threshold suffer box-state behavior due to the fixed boundary conditions we impose and are sensitive to the changes in the boundary-wall position. Hence, only the bound states below the threshold and resonance states above threshold are considered in our analysis. We ensure convergence of these states with respect to variation of both boundary position and grid size.

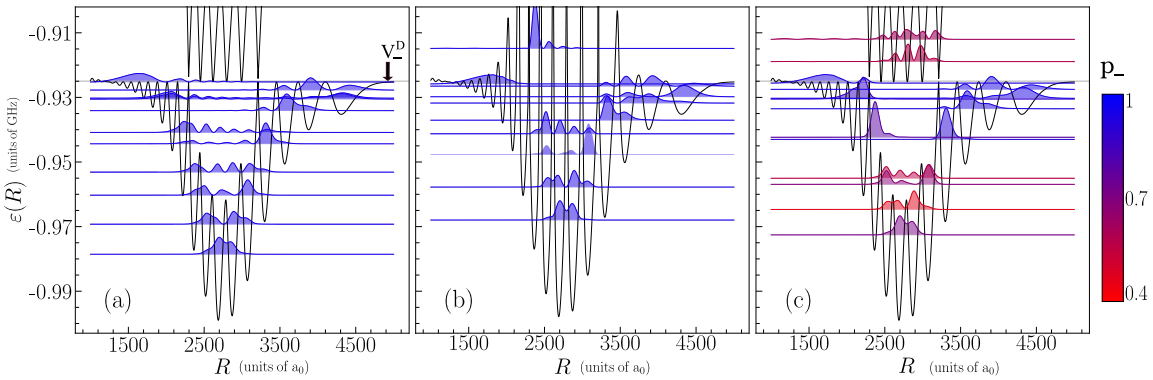

FIG. 4. Eigenspectrum of the ultralong-range sodium molecule for $n = 48$. Selected vibrational energy levels and probability densities of bound states correspond to (a) the V_- Born-Oppenheimer curve, (b) the V_-^b Born-Huang curve, and (c) the coupled-channel nonadiabatic system, with the adiabatic curves plotted for reference. Each vibrational level is color graded according to the electronic contribution by the $|\psi_-\rangle$ state, represented by the population p_-. The dissociation threshold of the V_- PEC, given by $V_-^D = -0.925$ GHz, is presented in (a).

IV. RESULTS AND DISCUSSION

In this section we discuss the electronic and vibronic spectral properties of the sodium ULRM. The principal quantum number $n = 48$ is used to illustrate the structure of the adiabatic PECs and derivative coupling terms, as it is representative of a strong vibronic interaction. We then proceed to discuss the complete vibronic spectra in comparison to the BO and the BH spectra and elaborate on the specific differences between them due to nonadiabatic interaction effects. The vibronic spectrum for $n = 43$ is also discussed, as it features less prominent vibronic coupling when compared to the $n = 48$ case.

A. Electronic structure

Figure 2 features the two-state adiabatic PECs $V_\pm$ determined for $n = 48$ (solid lines). At large R, close to the dissociation limit ($R \sim 4500\,a_0$), the PECs become nearly flat and match the energies of the hydrogenic manifold (V_+) and the d state (V_-), respectively. Inside the Rydberg orbit $R \leqslant 2n^2$, the $|\psi_+\rangle$ electronic state splits off of the hydrogenic manifold, causing the V_+ PEC to descend towards the V_- PEC and form narrow avoided crossings at $R \approx \{2295, 3210\}a_0$, where nonadiabatic couplings become large.

The exchange of the electronic-state character due to state mixing at avoided crossings is given by color grading the adiabatic PECs, with the R-dependent overlap of the adiabatic states with the d state. Corresponding to the mixing of electronic states, the $V_\pm$ PECs split away from $q(R)$ and $t(R)$ for $1700\,a_0 \leqslant R \leqslant 4300\,a_0$. For R values between the avoided crossings, V_- acquires a trilobite character, as is visible from the well structure of the PEC and the low-d-state contribution to $|\psi_-\rangle$. On the other hand, V_+, while being d-state dominant, has a significantly altered well structure. Note that, although $q(R)$ appears to be flat in the relevant energy scale, it does exhibit oscillatory structures of depth less than or equal to 6 MHz, significantly different in depth and structure from V_- for the complete R interval within which potential wells appear. The mixing of electronic states leads to the modification of transition dipole moments, facilitating the excitation of high-l states via two-photon transitions. We remark that the validity of our surfaces $V_\pm$ is confirmed by comparison to numerically obtained adiabatic PECs including atomic Rydberg

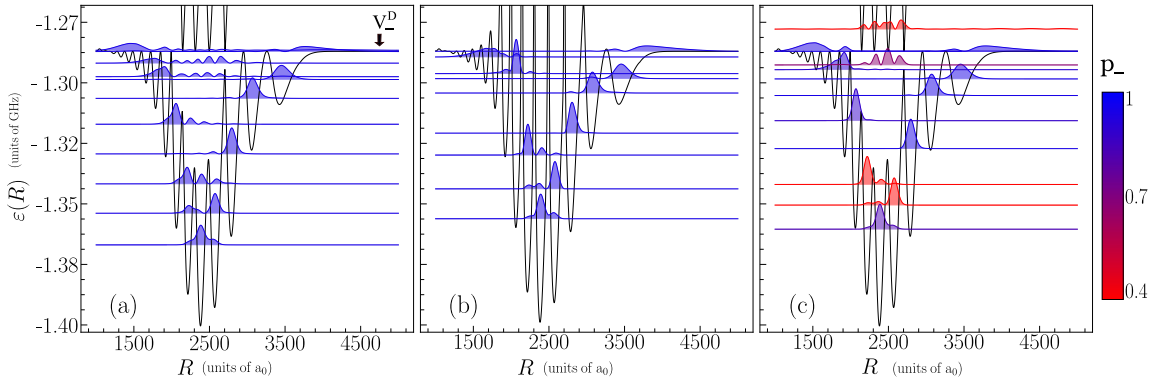

FIG. 5. Eigenspectrum of the ULRM for $n = 43$. Selected vibrational energy levels and probability densities of bound states correspond to (a) the V_- Born-Oppenheimer curve, (b) the V_-^b Born-Huang curve, and (c) the coupled-channel nonadiabatic system, with the adiabatic curves plotted for reference. Each vibrational level is color graded according to the electronic contribution by the $|\psi_-\rangle$ state, represented by the population p_-. The dissociation threshold of the V_- PEC, given by $V_-^D = -1.287$ GHz, is presented in (a).

states belonging to energetically neighboring n manifolds, as well as corresponding quantum-defect split states.

Furthermore, the single-color dashed lines are used to represent the diabatic PECs, corresponding to the trilobite state (red) and the d state (blue). Note that the diabatic curves cross each other at R values corresponding to the avoided crossings. This is expected, as the crossing of diabatic curves, given by the relation $t = q + \Delta$, minimizes the energy gap between the adiabatic PECs to $|V_+ - V_-| = \sqrt{4qt}$ [see Eq. (21)]. Due to the oscillatory nature of the d-state PEC, it is possible that the diabatic curves cross each other near the node of the $|nd0\rangle$ eigenstate. Such a coincidence would result in an extremely narrow avoided crossing, as is illustrated in Fig. 2 for the special case of $n = 48$.

Extending our analysis, if the $t = q + \Delta$ crossing exactly coincides with the node of $|nd0\rangle$, then q vanishes and the adiabatic PECs become degenerate, i.e., $|V_+ - V_-| = 0$. However, the von Neumann–Wigner noncrossing theorem prohibits an exact degeneracy of the PECs corresponding to electronic states of the same symmetry, in single-parameter (determined by R) diatomic systems [98]. We note that the use of the principal quantum number n, as a synthetic dimension [67], allows us to bypass the noncrossing theorem. This is facilitated by using Whittaker Coulomb functions as a replacement for the hydrogenic radial wave functions, for probing noninteger n [99,100]. The two-parameter diatomic system introduces the possibility of forming conical intersections at specific $\{n, R\}$ coordinates. Such CIs would result in complete degeneracy of the adiabatic potentials, representing $\{n, R\}$ values where the diabatic curves cross each other at exactly the node of $|nd0\rangle$. Hence, the width of the avoided crossings and consequently the strength of the nonadiabatic coupling is ascertained to be n dependent, corresponding to the proximity of the $\{n, R\}$ coordinate to a CI.

B. Nonadiabatic coupling

Figure 3 features the nonadiabatic couplings of the two adiabatic electronic states of the ULRM. Since the P matrix is anti-Hermitian, it suffices to analyze P_{12} $(=-P_{21})$ as off-diagonal coupling. Here P_{12} is divided by the reduced mass μ and a_0 so that it can be expressed in units of energy, as represented in Eq. (3). Similarly, Q_{11} and Q_{22} are divided by twice the reduced mass. The nonadiabatic couplings are then expressed in the same energy scale as the adiabatic PECs, allowing to us to compare their relative strengths as they appear in the vibrational TISE [see Eq. (3)] and consequently establish their importance in the calculation of the eigenspectrum.

The derivative off-diagonal coupling for $n = 48$ [see Fig. 3(a)] exhibits two near-singular peaks corresponding to the same R values as the narrow avoided crossings of the underlying PECs. At other R values, P_{12} also exhibits oscillatory structures with smaller amplitude, which are caused by the well structures of V_+ and V_- resulting in an oscillatory potential energy difference between them. The couplings vanish beyond $R > 4500\,a_0$ and $R < 1500\,a_0$, due to a negligible R-dependent state mixing. The second-order nonadiabatic couplings Q_{11} and Q_{22} are both dominated by the contribution from P_{12}, overpowering the derivative term in Eq. (7). Hence both diagonal terms feature near-singular peaks corresponding to the narrow avoided crossings, with negligible strength at other R values, on the displayed scale. The magnitude of the peaks in the nonadiabatic couplings far exceed the energy scale of the adiabatic potential energy curves near the avoided crossing, thereby causing the breakdown of the BO approximation. The strong contribution from the off-diagonal term which dominates the diagonal term implies that the BH approximation is also not applicable. Note that the magnitude and double-peak structure of the nonadiabatic couplings are specific to the $n = 48$ case, which allows the extremely narrow avoided crossings.

To further study the n dependence of nonadiabatic effects, we determine the magnitude of P_{12} over a parameter range of the principal quantum number [see Fig. 3(b)]. The linear structures formed by P_{12} stem from the fact that the length scale of the ULRM, and hence the position of the avoided crossings, scales as n^2. As explained before, these avoided crossings turn into CIs when the trilobite PEC crosses the d-state PEC, exactly at the zero of $|nd0\rangle$. Figure 3(b) features near-singular peaks for specific n values, which corresponds to the existence of such conical intersections accounting for synthetic dimensions. The $n = 48$ case is highlighted, as it is very close to two CIs, which explains the existence of two nearly degenerate avoided crossings and the double-peak structure of nonadiabatic couplings. Other integer n values which are not in the vicinity of a CI also feature prominent but less-peaked derivative couplings which correspond to their respective avoided crossings, which are wider compared to the $n = 48$ case.

C. Vibrational and vibronic spectra

We now perform a comparative analysis of the spectral features of the sodium ULRM, obtained using the BO approximation, the BH approximation, and the coupled-channel Hamiltonian for $n = 48$. Figures 4(a) and 4(b) show the vibrational probability densities of selected bound eigenstates shifted according to their energy eigenvalues calculated using the BO and BH approximations, respectively. Figure 4(c) shows the vibrational probability density of selected bound eigenstates of the coupled-channel Hamiltonian, obtained by tracing out the electronic degree of freedom, shifted according to their energy values. The probability densities are colored according p_-, the population of state $|\psi_-\rangle$. The black lines represent the V_-, V_+ PECs in Figs. 4(a) and 4(c) and the BH corrected V_-^b PEC in Fig. 4(b).

We observe that the vibronic eigenvalues exhibit a significant positive shift in energy when compared to the vibrational eigenvalues obtained using the BO approximation. For $n = 48$, the full vibronic system possesses a ground-state shifted approximately 6 MHz higher in energy than the BO ground state and exhibits negligible energy shifts for bound states near the continuum threshold. The energy gaps between the eigenvalues of the BO system fail to mimic the energy gaps exhibited by the coupled-channel nonadiabatic system. The Born-Huang correction shifts the vibrational ground state approximately 11 MHz higher in energy than the BO ground state, effectively placing it above the first excited state of the BO system and above the ground state of the

coupled-channel system. The higher excited states near the continuum also show significant positive-energy shifts (approximately 4 MHz) between the BO and the BH approximations. The overcorrection in energy values, due to the BH correction, is a result of including only the positive diagonal terms without considering the level repulsion introduced by the off-diagonal terms.

We also observe pronounced differences in the vibrational probability densities obtained within the three models. The vibrational ground state associated with the V_- PEC is delocalized between several wells (2500 a_0–3300 a_0). The ground state belonging to the BH and exact spectra, although similar in density profile, is more localized. Subsequent excited states belonging to the BH and exact spectra, while exhibiting different density profiles, also show more localized behavior. For example, the fourth excited BO state in Fig. 4(a) is delocalized in R over the entire of the V_- PEC at the relevant energy scale. In contrast, the corresponding coupled states presented in Fig. 4(c) exhibit localization in R over the span of a single potential well. Similar effects of localization are also clearly visible in the fifth and seventh excited states of the system. The higher potential barrier introduced between the potential wells by the diagonal BH correction can be viewed as an explanation for vibrational localization in the BH spectrum. However, the vibronic spectrum has a significantly altered probability distribution that is not explained by the diagonal correction alone. Interestingly, the fourth and fifth excited states of the vibronic spectrum are localized in two separate outer wells, allowing them to be nearly degenerate. Note that below the continuum threshold of -0.925 GHz, the BO and BH spectra contain states with purely ψ_- character. Counterintuitively, we observe significant state mixing for the first three excited states of the coupled system, even though they appear to be well localized in the V_- PEC. This indicates strong nonadiabatic couplings between the two closed channels, well below the continuum limit.

A key observation to be made is the existence of nonadiabatic resonance states visible above the V_- dissociation threshold. For energies above -0.925 GHz, the $n = 48$ V_- adiabatic PEC corresponds to an open channel, featuring only continuum states. However, in the complete vibronic picture [Fig. 4(c)], bound states are observed at energies of approximately -0.919 and -0.912 GHz, with significant state mixing (determined by color value). The vibrational probability density of these bound states is localized in the potential energy wells of V_+, but is localized much below the ground state of V_+; hence, it cannot be interpreted to belong to either one of the single channels. The BH spectrum does contain a bound state of energy -0.915 GHz localized in the V_-^b PEC, but this does not compare in energy value or probability density to the aforementioned resonance states. The bound states are hence explained as scattering resonances due to the off-diagonal nonadiabatic coupling between an open channel (limited to V_-) and a closed channel (limited to V_+).

Figure 5 features the vibrational and vibronic spectra, as an extension of the previous case study, for $n = 43$, following the same structure and description as in Fig. 4. The $n = 43$ case is of comparative value, as the system is not in the vicinity of a CI [Fig. 3(b)] as opposed to the $n = 48$ case. The PECs features a much wider avoided crossing ($R \sim 2700\, a_0$) as portrayed in Fig. 5, and the differential couplings, while prominent, are not as peaked as in the $n = 48$ case. The ground states of the BH spectrum and the exact spectrum are shifted by approximately 11 MHz and 6.5 MHz, respectively, relative to the BO ground state. The positive-energy shift due to the nonadiabatic coupling does not vary significantly between the $n = 43$ and $n = 48$ cases. However, the deeper wells of the $n = 43$ PECs ensure that the energy splitting is of less relative importance than for the $n = 48$ case. The first two excited eigenstates of the exact spectrum portray significant state mixing and the nonadiabatic bound states are more localized than the BO states. The BH states near the continuum threshold show lower-energy splitting than the $n = 48$ case, which is associated with the fact that $n = 43$ has a less prominent diagonal correction, due to its less prominent nonadiabatic coupling. Much like the previous case, the vibronic interaction does introduce the radial localization of states for $n = 43$. The fourth, fifth, and eighth excited states of the BO spectrum are all delocalized over multiple wells, in contrast to the corresponding well-localized nonadiabatic states. As a final note in our comparison, a scattering resonance state with no BO or BH counterpart is observed at an energy of approximately -1.278 GHz, well above the continuum threshold of -1.287 GHz.

It is worth noting that although the nonadiabatic couplings are highly n dependent, the behavior of the diabatic curves does not vary significantly over n. Hence the positive-energy shifts (on the order of megahertz), state localization, and existence of resonance states for the exact spectrum are all commonly observed for $30 \leqslant n \leqslant 60$. The pattern of n-dependent singularities [Fig. 3(b)] are also repeated regularly for $30 \leqslant n \leqslant 60$. However, as the energies of the PECs scale as n^{-3}, the contribution of nonadiabatic interaction effects to the complete molecular spectra becomes more important for higher-n values.

V. CONCLUSION AND OUTLOOK

We have investigated nonadiabatic and vibronic interaction effects in the sodium ultralong-range molecule, using the vibronic coupling between states of trilobite and d-state character. The oscillatory nature of the trilobite and d-state PECs, along with the specific quantum defect splitting of sodium, ensures the formation of avoided crossings for a range of n values. We observed that the avoided crossing between the adiabatic PECs introduce significant nonadiabatic couplings that can behave like a singularity for specific n, which is associated with the existence of CIs in synthetic dimensions. Irrespective of the form of the derivative couplings, the exact spectra feature pronounced differences from the BO spectra, including megahertz-scale positive-energy shifts in eigenvalues, localized probability densities, and the existence of scattering resonance states near the avoided crossings, with no adiabatic counterpart. While the Born-Huang correction does partially explain the energy shift and the state localization, it cannot account for the exact spectra and the resonance states. Hence, our results confirm that a coupled-channel approach is necessary to study the vibronic spectra of sodium ULRMs, irrespective of the corresponding principal quantum number n.

A direct extension of our present work would be to include the *p*-wave scattering terms as well as fine and hyperfine interactions. Inclusion of these terms, although representing a challenge, can help obtain results that are empirically comparable and be further developed to study nonadiabatic effects in spin interacting systems. Nonadiabatic interactions in such systems might give insight into spin-changing and *l*-changing collision dynamics.

Furthermore, the present study of ULRMs also offers the possibility for research opportunities in nonadiabatic wave-packet dynamics. Notably, the introduction of an electric field breaks the spherical symmetry of the system and facilitates the existence of conical intersections in spatial dimensions. This provides ample opportunity to probe and observe nonadiabatic dynamics near CIs, on timescales of microseconds and distances of the order of micrometers, which are accessible in present-day cold-atom laboratories. Finally, explorations of ULRMs to date have been focusing on heavier molecules formed by the species K, Rb, Cs, and Sr [35,49,53,101]. Here the ability to concoct these molecules allows for a probing of vibronic interaction effects in heavier ULRMs. In addition, corresponding experiments with (ultra)cold sodium clouds would allow one to address the presently investigated ULRMs [102,103]. Hence, we justify the utility of lighter molecules based on Na, as they feature strong nonadiabatic effects and a rich vibronic structure and promote interest in the experimental study of sodium Rydberg molecules.

ACKNOWLEDGMENTS

We acknowledge support from the Deutsche Forschungsgemeinschaft (DFG) within the priority program "Giant Interactions in Rydberg Systems" (DFG SPP 1929 GiRyd Project No. SCHM 885/30-2). R.S. is grateful to Dan Bosworth for beneficial discussions.

[1] T. F. Gallagher, *Rydberg Atoms* (Cambridge University Press, Cambridge, 1994).
[2] N. Šibalić and C. S. Adams, *Rydberg Physics* (IOP, Bristol, 2018).
[3] M. Saffman, T. G. Walker, and K. Mølmer, Rev. Mod. Phys. **82**, 2313 (2010).
[4] M. Saffman, J. Phys. B **49**, 202001 (2016).
[5] A. Browaeys and T. Lahaye, Nat. Phys. **16**, 132 (2020).
[6] D. Bluvstein, H. Levine, G. Semeghini, T. T. Wang, S. Ebadi, M. Kalinowski, A. Keesling, N. Maskara, H. Pichler, M. Greiner, V. Vuletić, and M. D. Lukin, Nature (London) **604**, 451 (2022).
[7] T. M. Graham, Y. Song, J. Scott, C. Poole, L. Phuttitarn, K. Jooya, P. Eichler, X. Jiang, A. Marra, B. Grinkemeyer, M. Kwon, M. Ebert, J. Cherek, M. T. Lichtman, M. Gillette, J. Gilbert, D. Bowman, T. Ballance, C. Campbell, E. D. Dahl *et al.*, Nature (London) **604**, 457 (2022).
[8] J. A. Sedlacek, A. Schwettmann, H. Kübler, R. Löw, T. Pfau, and J. P. Shaffer, Nat. Phys. **8**, 819 (2012).
[9] H. Fan, S. Kumar, J. Sedlacek, H. Kübler, S. Karimkashi, and J. P. Shaffer, J. Phys. B **48**, 202001 (2015).
[10] J. A. Gordon, C. L. Holloway, A. Schwarzkopf, D. A. Anderson, S. Miller, N. Thaicharoen, and G. Raithel, Appl. Phys. Lett. **105**, 024104 (2014).
[11] M. Zeppenfeld, Europhys. Lett. **118**, 13002 (2017).
[12] S. Patsch, M. Zeppenfeld, and C. P. Koch, J. Phys. Chem. Lett. **13**, 10728 (2022).
[13] J. Zou and S. D. Hogan, Phys. Rev. A **106**, 043111 (2022).
[14] O. Firstenberg, C. S. Adams, and S. Hofferberth, J. Phys. B **49**, 152003 (2016).
[15] T. Peyronel, O. Firstenberg, Q.-Y. Liang, S. Hofferberth, A. V. Gorshkov, T. Pohl, M. D. Lukin, and V. Vuletić, Nature (London) **488**, 57 (2012).
[16] O. Firstenberg, T. Peyronel, Q.-Y. Liang, A. V. Gorshkov, M. D. Lukin, and V. Vuletić, Nature (London) **502**, 71 (2013).
[17] A. Paris-Mandoki, C. Braun, J. Kumlin, C. Tresp, I. Mirgorodskiy, F. Christaller, H. P. Büchler, and S. Hofferberth, Phys. Rev. X **7**, 041010 (2017).
[18] C. H. Greene, A. S. Dickinson, and H. R. Sadeghpour, Phys. Rev. Lett. **85**, 2458 (2000).
[19] C. Boisseau, I. Simbotin, and R. Côté, Phys. Rev. Lett. **88**, 133004 (2002).
[20] S. Hollerith, J. Zeiher, J. Rui, A. Rubio-Abadal, V. Walther, T. Pohl, D. M. Stamper-Kurn, I. Bloch, and C. Gross, Science **364**, 664 (2019).
[21] K. R. Overstreet, A. Schwettmann, J. Tallant, D. Booth, and J. P. Shaffer, Nat. Phys. **5**, 581 (2009).
[22] A. Duspayev, X. Han, M. A. Viray, L. Ma, J. Zhao, and G. Raithel, Phys. Rev. Res. **3**, 023114 (2021).
[23] M. Deiß, S. Haze, and J. Hecker Denschlag, Atoms **9**, 34 (2021).
[24] D. J. Bosworth, F. Hummel, and P. Schmelcher, Phys. Rev. A **107**, 022807 (2023).
[25] A. Duspayev and G. Raithel, Phys. Rev. A **105**, 012810 (2022).
[26] N. Zuber, V. S. V. Anasuri, M. Berngruber, Y.-Q. Zou, F. Meinert, R. Löw, and T. Pfau, Nature (London) **605**, 453 (2022).
[27] Y.-Q. Zou, M. Berngruber, V. S. V. Anasuri, N. Zuber, F. Meinert, R. Löw, and T. Pfau, Phys. Rev. Lett. **130**, 023002 (2023).
[28] W. Li, T. Pohl, J. M. Rost, S. T. Rittenhouse, H. R. Sadeghpour, J. Nipper, B. Butscher, J. B. Balewski, V. Bendkowsky, R. Löw, and T. Pfau, Science **334**, 1110 (2011).
[29] D. Booth, S. T. Rittenhouse, J. Yang, H. R. Sadeghpour, and J. P. Shaffer, Science **348**, 99 (2015).
[30] M. A. Bellos, R. Carollo, J. Banerjee, E. E. Eyler, P. L. Gould, and W. C. Stwalley, Phys. Rev. Lett. **111**, 053001 (2013).
[31] N. Y. Du and C. H. Greene, Phys. Rev. A **36**, 971 (1987).
[32] E. L. Hamilton, C. H. Greene, and H. R. Sadeghpour, J. Phys. B **35**, L199 (2002).
[33] T. Niederprüm, O. Thomas, T. Eichert, C. Lippe, J. Pérez-Ríos, C. H. Greene, and H. Ott, Nat. Commun. **7**, 12820 (2016).
[34] P. Giannakeas, M. T. Eiles, F. Robicheaux, and J. M. Rost, Phys. Rev. Lett. **125**, 123401 (2020).
[35] V. Bendkowsky, B. Butscher, J. Nipper, J. P. Shaffer, R. Löw, and T. Pfau, Nature (London) **458**, 1005 (2009).

[36] J. D. Whalen, S. K. Kanungo, R. Ding, M. Wagner, R. Schmidt, H. R. Sadeghpour, S. Yoshida, J. Burgdörfer, F. B. Dunning, and T. C. Killian, Phys. Rev. A **100**, 011402(R) (2019).

[37] F. Engel, T. Dieterle, F. Hummel, C. Fey, P. Schmelcher, R. Löw, T. Pfau, and F. Meinert, Phys. Rev. Lett. **123**, 073003 (2019).

[38] R. Schmidt, H. R. Sadeghpour, and E. Demler, Phys. Rev. Lett. **116**, 105302 (2016).

[39] J. Sous, H. R. Sadeghpour, T. C. Killian, E. Demler, and R. Schmidt, Phys. Rev. Res. **2**, 023021 (2020).

[40] M. T. Eiles and C. H. Greene, Phys. Rev. A **95**, 042515 (2017).

[41] C. Fey, F. Hummel, and P. Schmelcher, Mol. Phys. **118**, e1679401 (2020).

[42] D. A. Anderson, S. A. Miller, and G. Raithel, Phys. Rev. A **90**, 062518 (2014).

[43] I. Lesanovsky, P. Schmelcher, and H. R. Sadeghpour, J. Phys. B **39**, L69 (2006).

[44] M. Kurz and P. Schmelcher, J. Phys. B **47**, 165101 (2014).

[45] F. Hummel, C. Fey, and P. Schmelcher, Phys. Rev. A **99**, 023401 (2019).

[46] F. Hummel, K. Keiler, and P. Schmelcher, Phys. Rev. A **103**, 022827 (2021).

[47] M. Kurz and P. Schmelcher, Phys. Rev. A **88**, 022501 (2013).

[48] J. P. Shaffer, S. T. Rittenhouse, and H. R. Sadeghpour, Nat. Commun. **9**, 1965 (2018).

[49] B. J. DeSalvo, J. A. Aman, F. B. Dunning, T. C. Killian, H. R. Sadeghpour, S. Yoshida, and J. Burgdörfer, Phys. Rev. A **92**, 031403(R) (2015).

[50] J. D. Whalen, S. K. Kanungo, Y. Lu, S. Yoshida, J. Burgdörfer, F. B. Dunning, and T. C. Killian, Phys. Rev. A **101**, 060701(R) (2020).

[51] T. Schmid, C. Veit, N. Zuber, R. Löw, T. Pfau, M. Tarana, and M. Tomza, Phys. Rev. Lett. **120**, 153401 (2018).

[52] T. Niederprüm, O. Thomas, T. Eichert, and H. Ott, Phys. Rev. Lett. **117**, 123002 (2016).

[53] M. Peper and J. Deiglmayr, Phys. Rev. Lett. **126**, 013001 (2021).

[54] D. A. Anderson, S. A. Miller, and G. Raithel, Phys. Rev. Lett. **112**, 163201 (2014).

[55] K. S. Kleinbach, F. Meinert, F. Engel, W. J. Kwon, R. Löw, T. Pfau, and G. Raithel, Phys. Rev. Lett. **118**, 223001 (2017).

[56] M. Schlagmüller, T. C. Liebisch, F. Engel, K. S. Kleinbach, F. Böttcher, U. Hermann, K. M. Westphal, A. Gaj, R. Löw, S. Hofferberth, T. Pfau, J. Pérez-Ríos, and C. H. Greene, Phys. Rev. X **6**, 031020 (2016).

[57] F. Böttcher, A. Gaj, K. M. Westphal, M. Schlagmüller, K. S. Kleinbach, R. Löw, T. C. Liebisch, T. Pfau, and S. Hofferberth, Phys. Rev. A **93**, 032512 (2016).

[58] F. Camargo, J. D. Whalen, R. Ding, H. R. Sadeghpour, S. Yoshida, J. Burgdörfer, F. B. Dunning, and T. C. Killian, Phys. Rev. A **93**, 022702 (2016).

[59] B. Butscher, V. Bendkowsky, J. Nipper, J. B. Balewski, L. Kukota, R. Löw, T. Pfau, W. Li, T. Pohl, and J. M. Rost, J. Phys. B **44**, 184004 (2011).

[60] M. Born and R. Oppenheimer, Ann. Phys. (Leipzig) **389**, 457 (1927).

[61] A. Duspayev, A. Shah, and G. Raithel, New J. Phys. **24**, 053043 (2022).

[62] H. Köuppel, W. Domcke, and L. S. Cederbaum, in *Advances in Chemical Physics*, edited by I. Prigogine and S. A. Rice, (Wiley, New York, 1984), Vol. 57, pp. 59–246.

[63] F. Agostini and B. F. E. Curchod, Wiley Interdiscip. Rev. Comput. Mol. Sci. **9**, e1417 (2019).

[64] M. Baer, *Beyond Born-Oppenheimer: Electronic Nonadiabatic Coupling Terms and Conical Intersections* (Wiley, New York, 2006).

[65] D. R. Yarkony, Rev. Mod. Phys. **68**, 985 (1996).

[66] S. Matsika and P. Krause, Annu. Rev. Phys. Chem. **62**, 621 (2011).

[67] F. Hummel, M. T. Eiles, and P. Schmelcher, Phys. Rev. Lett. **127**, 023003 (2021).

[68] C. Arnold, O. Vendrell, R. Welsch, and R. Santra, Phys. Rev. Lett. **120**, 123001 (2018).

[69] N. Mabrouk, W. Zrafi, and H. Berriche, Mol. Phys. **118**, e1605098 (2020).

[70] T. J. Martinez, Nature (London) **467**, 412 (2010).

[71] H. Köppel, W. Domcke, and L. S. Cederbaum, *Stochasticity and Intramolecular Redistribution of Energy* (Springer Netherlands, Dordrecht, 1987), pp. 217–231.

[72] H. A. Jahn, E. Teller, and F. G. Donnan, Proc. R. Soc. A **161**, 220 (1937).

[73] H. C. Longuet-Higgins, U. Öpik, M. H. L. Pryce, and R. A. Sack, Proc. R. Soc. A **244**, 1 (1958).

[74] M. F. Herman, J. Chem. Phys. **81**, 754 (1984).

[75] M. Barbatti, Wiley Interdiscip. Rev. Comput. Mol. Sci. **1**, 620 (2011).

[76] M. Barbatti, A. J. A. Aquino, J. J. Szymczak, D. Nachtigallová, P. Hobza, and H. Lischka, Proc. Natl. Acad. Sci. USA **107**, 21453 (2010).

[77] H. Kang, K. T. Lee, B. Jung, Y. J. Ko, and S. K. Kim, J. Am. Chem. Soc. **124**, 12958 (2002).

[78] B. G. Levine and T. J. Martínez, Annu. Rev. Phys. Chem. **58**, 613 (2007).

[79] D. Polli, P. Altoè, O. Weingart, K. M. Spillane, C. Manzoni, D. Brida, G. Tomasello, G. Orlandi, P. Kukura, R. A. Mathies, M. Garavelli, and G. Cerullo, Nature (London) **467**, 440 (2010).

[80] L. Hammarström and S. Styring, Philos. Trans. R. Soc. B **363**, 1283 (2008).

[81] S. Hollerith, J. Rui, A. Rubio-Abadal, K. Srakaew, D. Wei, J. Zeiher, C. Gross, and I. Bloch, Phys. Rev. Res. **3**, 013252 (2021).

[82] F. Hummel, P. Schmelcher, and M. T. Eiles, Phys. Rev. Res. **5**, 013114 (2023).

[83] M. Born and K. Huang, *Dynamical Theory of Crystal Lattices* (Oxford University Press, Oxford, 1954).

[84] U. Manthe and H. Köppel, J. Chem. Phys. **93**, 345 (1990).

[85] W. Domcke, D. R. Yarkony, and H. Köppel, *Conical Intersections* (World Scientific, Singapore, 2004).

[86] T. Pacher, L. S. Cederbaum, and H. Köppel, J. Chem. Phys. **89**, 7367 (1988).

[87] E. Fermi, Nuovo Cim. **11**, 157 (1934).

[88] A. Omont, J. Phys. (Paris) **38**, 1343 (1977).

[89] M. T. Eiles, Phys. Rev. A **98**, 042706 (2018).

[90] E. Karule, Phys. Lett. **15**, 137 (1965).

[91] W. F. Holmgren, M. C. Revelle, V. P. A. Lonij, and A. D. Cronin, Phys. Rev. A **81**, 053607 (2010).
[92] J. Mitroy, M. S. Safronova, and C. W. Clark, J. Phys. B **43**, 202001 (2010).
[93] C. R. Ekstrom, J. Schmiedmayer, M. S. Chapman, T. D. Hammond, and D. E. Pritchard, Phys. Rev. A **51**, 3883 (1995).
[94] C. J. Lorenzen and K. Niemax, Phys. Scr. **27**, 300 (1983).
[95] G. A. Worth and L. S. Cederbaum, Annu. Rev. Phys. Chem. **55**, 127 (2004).
[96] Z. Top and M. Baer, Chem. Phys. **10**, 95 (1975).
[97] G. C. Groenenboom and H. M. Buck, J. Chem. Phys. **92**, 4374 (1990).
[98] J. von Neumann and E. P. Wigner, *The Collected Works of Eugene Paul Wigner* (Springer, Berlin, 1993), Pt. A, pp. 291–293.
[99] M. T. Eiles, J. Phys. B **52**, 113001 (2019).
[100] J. Wang and R. Côté, Phys. Rev. Res. **2**, 023019 (2020).
[101] C. Vadla, V. Horvatic, and K. Niemax, Phys. Rev. A **80**, 052506 (2009).
[102] S. Banik, M. G. Galan, H. Sosa-Martinez, M. J. Anderson, S. Eckel, I. B. Spielman, and G. K. Campbell, Phys. Rev. Lett. **128**, 090401 (2022).
[103] T. Świsłocki, M. Gajda, M. Brewczyk, and P. Deuar, Sci. Rep. **11**, 6441 (2021).